



# Technical note: Isolating methane emissions from animal feeding operations in an interfering location

Megan E. McCabe<sup>1</sup>, Ilana B. Pollack<sup>2</sup>, Emily V. Fischer<sup>2</sup>, and Dana R. Caulton<sup>1</sup>

<sup>1</sup>Department of Atmospheric Science, University of Wyoming, Laramie, WY, 82071, USA

<sup>2</sup>Department of Atmospheric Science, Colorado State University, Fort Collins, Colorado, 80523, USA

**Correspondence:** Dana R. Caulton (dcaulton@uwyo.edu)

**Abstract.** Agriculture emissions, including those from cattle and dairy concentrated animal feeding operations (CAFOs), make up a large portion of the United States' total greenhouse gas emissions. However, many CAFOs reside in areas where methane (CH<sub>4</sub>) from oil and natural gas complicates the quantification of CAFO emissions. Traditional approaches to quantify emissions in such regions often relied on inventory subtraction of other known sources. We compare the results of two approaches to attribute a CAFO CH<sub>4</sub> emission rate from an aircraft mass-balance derived CH<sub>4</sub> emission rate. These methods make use of the CH<sub>4</sub>, ethane (C<sub>2</sub>H<sub>6</sub>) and ammonia (NH<sub>3</sub>) mixing ratio data collected simultaneously in-flight downwind of CAFOs in northeastern Colorado. The first approach, subtraction method, is similar to inventory subtraction except the amount to be removed is derived from the observed C<sub>2</sub>H<sub>6</sub> to CH<sub>4</sub> ratio rather than an inventory estimate. The results from this approach showed high uncertainty, primarily due to how error propagates through subtraction. Alternatively, multivariate regression (MVR) can be used to estimate CAFO CH<sub>4</sub> emissions using the NH<sub>3</sub> emission rate and an NH<sub>3</sub> to CH<sub>4</sub> ratio. These results showed significantly less uncertainty. We identified criteria to determine the best attribution method; these criteria can support attribution in other regions. The final emissions estimates for the CAFO presented here were 23 (±5) g CH<sub>4</sub> head<sup>-1</sup> hr<sup>-1</sup> and 22 (±4) g NH<sub>3</sub> head<sup>-1</sup> hr<sup>-1</sup>. These estimates are significantly higher than the US EPA inventory and previous studies highlighting the need for more measurements of CH<sub>4</sub> and NH<sub>3</sub> emission rates.

## 1 Introduction

Livestock produce large amounts of greenhouse gases (GHG) and reactive nitrogen species, including methane (CH<sub>4</sub>) and ammonia (NH<sub>3</sub>), through enteric fermentation and waste generation. Ruminant animals (e.g. cattle, buffalo, sheep, goats, and camels) constitute a significant source of CH<sub>4</sub> as their digestive systems break down coarse plant material through microbial fermentation in their rumen stomach (large frontal stomach) and subsequently release the produced gas (CH<sub>4</sub>). From 1990 to 2019, CH<sub>4</sub> emissions from enteric fermentation grew 8.4%, making agriculture the largest source of US CH<sub>4</sub> anthropogenic emission in 2020 (EPA, 2022). Waste and manure management are also significant emission sources of CH<sub>4</sub> and NH<sub>3</sub>. Together enteric fermentation and manure management account for more than 30% of US anthropogenic CH<sub>4</sub> emissions (EPA, 2022)(Maasackers et al., 2016; EPA, 2022). CH<sub>4</sub> is a crucial GHG due to its high global warming potential (Myhre et al., 2013; Moumen et al., 2016; Smith et al., 2021).



25 Large uncertainty remains around the magnitude of livestock emissions. Beef and dairy cattle are confined to feedlots where they are fed and kept in tight areas to process the animals efficiently. These feedlots are known as concentrated animal feeding operations (CAFOs). The compactness of CAFOs has been shown to create significant emissions (Golston et al., 2020; Hacker et al., 2016; Eilerman et al., 2016; Staebler et al., 2009). However, observations indicated large variability in these CH<sub>4</sub> emissions, which creates uncertainty in cumulative estimates of agricultural emissions (Golston et al., 2020). There are many  
30 different factors determining the amount of CH<sub>4</sub> released from enteric fermentation and manure management and practices may vary from farm to farm (EPA, 2022; Maasackers et al., 2016). However, interfering sources of CH<sub>4</sub> and NH<sub>3</sub>, such as oil and natural gas (ONG), waste pools, and landfills, etc., may also complicate measurements from individual CAFOs. Improving the methodology for isolating CAFO signals from other interfering sources will allow more accurate measurements and provide new information to constrain greenhouse gas emissions from the agriculture sector.

35 When CH<sub>4</sub> concentration data are used alone for emissions quantification in regions with multiple CH<sub>4</sub> sources there is not enough information to distinguish the contributing sources. However, previous studies have attributed CH<sub>4</sub> emissions in complicated regions using a variety of methods. A few examples include attribution by subtracting inventory data (Caulton et al., 2014; Peischl et al., 2015, 2018), collecting ground based isotope data to attribute CH<sub>4</sub> signals (Townsend-Small et al., 2016), using C<sub>2</sub>H<sub>6</sub> as a tracer to subtract or attribute the ONG fraction, (Mielke-Maday et al., 2019), and using multivariate  
40 regression (MVR) using independent gas tracers to attribute sectors (Kille et al., 2019; Pollack et al., 2022).

There are many considerations when determining which attribution method is most appropriate, and often attribution is done based on the data available rather than the ideal methodology. Attribution using the subtraction of a value determined by inventory or calculated ratio is best done for larger regions due to the variability of emissions from individual sources. For ONG, individual sites can release different amounts of CH<sub>4</sub> and ethane (C<sub>2</sub>H<sub>6</sub>) compared to other wells and compressors  
45 (Yacovitch et al., 2014; Zimmerle et al., 2022). When quantifying emissions in a small region (as in this work), an estimate of emissions from each type of ONG source or a local C<sub>2</sub>H<sub>6</sub>:CH<sub>4</sub> ratio near the CAFO is required to accurately separate the CH<sub>4</sub> emissions into contributions from the CAFO and nearby ONG activities.

Another concern with using a tracer like C<sub>2</sub>H<sub>6</sub> in isolation to estimate the contribution of ONG is that in complicated regions individual CH<sub>4</sub> signals become mixed, making it possible that the observed ratio by aircraft is not representative of  
50 the original ratio at the ground. This is the theory behind tracer release, for example, where a tracer gas is released at a known rate near a source of interest and used to back out the source emission rate (Roscioli et al., 2015). The added gas does not have to be introduced exactly at the source emission point (which may be unknown), provided sampling occurs far enough downwind where the species are well mixed. Typically this means the tracer gas must be released within 100 m of the source and measured >500 m downwind (Roscioli et al., 2015). For airborne data there are many situations where we would  
55 expect signals to be mixed complicating the use of airborne ratio analysis. Townsend-Small et al. (2016) circumvented this by combining ground-based isotope ratios (which show distinct ratios for particular sources) with aircraft data (which showed only one ratio). However, because they used a single isotope ratio there is large uncertainty in their results stemming from the single isotope ratio that must be attributed to multiple contribution signals (1 equation, multiple unknowns). This is similar to



the difficulties that Smith et al. (2015) encountered using  $C_2H_6$  as a tracer in a complicated region with multiple  $C_2H_6:CH_4$  ratios.

On the other hand, an approach like MVR, which makes use of multiple tracer gases, requires sufficient data and is subject to its own sensitivities (Kille et al., 2019). MVR is best used when there are multiple tracer gases that can be treated as independent variables and one dependent variable (i.e.  $CH_4$ ). The more independent variables that are included, the more data is needed to produce statistically significant results. MVR can also be used in situations where it is not appropriate, for example in a region where one might assume there are multiple sources, but in reality there are not.

Here we demonstrate methodology to isolate and quantify emission rates for individual CAFOs in the northeastern Colorado Front Range (NCFR) using airborne measurements of  $CH_4$ ,  $C_2H_6$ , and  $NH_3$ . We investigated two methods for CAFO  $CH_4$  emission isolation: 1) a subtraction method using the  $C_2H_6:CH_4$  ratio and 2) a MVR method using  $CH_4$ ,  $C_2H_6$  and  $NH_3$ . This study focuses on the NCFR, where there is a high density of large CAFOs. Figure 1 shows a map of the NCFR with CAFOs for beef cattle, dairy cattle, chickens, sheep, and swine in the area. The area is dominated by beef cattle and dairy CAFOs. However, the NCFR contains a large mixture of  $CH_4$  emissions, due to the high production of ONG. In this region, prior estimates indicate that natural gas accounts for 38.5% of the state-wide  $CH_4$  emissions, while agriculture accounts for 22.3% of the state-wide  $CH_4$  emissions (Arnold et al., 2014). The NCFR is home to Denver-Julesburg Basin (DJB), with over 52,000 ONG wells, and has an abundance of compressors and processing plants; many of which are in close proximity to CAFOs (Higley and Cox, 2007).

## 2 Materials and Methods

### 2.1 Data Collection

This study was conducted in the NCFR near Greeley, CO; the analysis includes data collected over Weld, Morgan, Logan, Larimer, and Washington counties. There are many CAFOs within these five counties with an area wide maximum capacity >1,000,000 heads of cattle (United States Department of Agriculture [USDA], 2018). This study used the University of Wyoming King Air (UWKA), which is a relatively small research aircraft capable of flying at low altitudes (100 m AGL) and slow flight speeds (95 m/s). The UWKA is a national aircraft research facility owned and operated by the University of Wyoming. Flights departed from and returned to the Laramie Airport in Laramie, Wyoming (KLAR). Three flights were performed in November 2019, departing around 12:00 Mountain Standard Time (MST) and lasting 2-4 hours.

The UWKA was instrumented to measure  $CH_4$ ,  $NH_3$ , and  $C_2H_6$  mixing ratios. A Picarro G2401-m flight-ready analyzer measured  $CH_4$ , carbon monoxide (CO), carbon dioxide ( $CO_2$ ), and water vapor ( $H_2O$ ) at 0.25 Hz through infrared cavity ring-down spectroscopy (Crosson, 2008). This model and other Picarro models were tested previously and found to be stable and suitable for airborne field measurements (Richardson et al., 2012). Two separate Aerodyne commercial quantum-cascade tunable infrared laser direct absorption spectrometers (QC-TILDAS) measured  $NH_3$  and  $C_2H_6$ . These instruments are described in detail in Yacovitch et al. (2014), Pollack et al. (2019), and Pollack et al. (2022).  $NH_3$  measurements are collected at 10 Hz and averaged to 1 Hz for reporting and this analysis;  $C_2H_6$  measurements are collected and reported at 1 Hz. All chemical

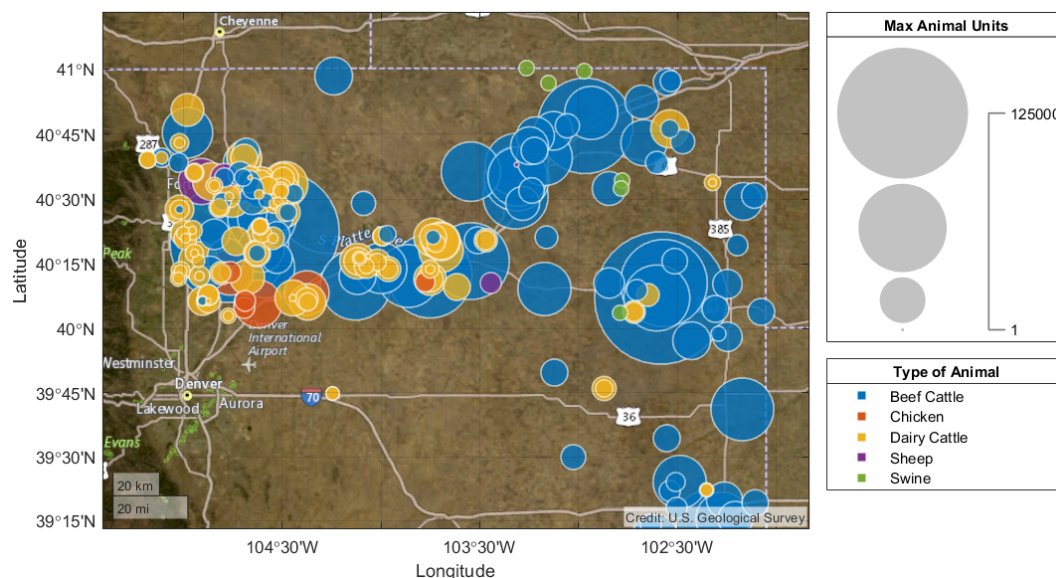


**Figure 1.** Map of Northeastern Colorado. Beef cattle (blue), dairy cattle (yellow), chicken (orange), sheep (purple), and swine (green) CAFOs are sized by max animal units. Animal units are equivalent to 1 live beef cattle such that 1 head of beef cattle = 0.7 dairy cattle = 2.5 swine = 10 sheep = 100 poultry. Note that the maximum animal units represent the maximum animal capacity of a given facility and not necessarily the actual number of animals present at that facility at the time of sampling. CAFO data as of 2017 registered with the Colorado Department of Public Health & Environment (CDPHE, 2017).

data was adjusted for time lag between instruments and further averaged to 0.25 Hz for emission calculations. Instruments were calibrated on the ground before and after flights. Instrument zeros were routinely measured in flight by overblowing the instrument inlets with a bottled source of synthetic “zero” air. Other in-situ measurements from the UWKA standard instrument package included pressure, temperature, three-dimension winds, GPS position, aircraft altitude, and heading.

## 2.2 Flight Patterns

Flights were designed to identify the best flight patterns to simultaneously quantify CH<sub>4</sub> and NH<sub>3</sub> emission fluxes, CH<sub>4</sub> to NH<sub>3</sub> ratios, and NH<sub>3</sub> deposition downwind of CAFOs. Prior to each flight, forecast meteorology was used to identify the ideal CAFOs to sample based on prevailing wind direction, isolation from other CAFO plumes, and other logistical constraints (e.g. proximity to urban areas, towers and airports). Once airborne, the pilot conducted a vertical profile to characterize the mixed boundary layer (MBL). Selected CAFOs were located by coordinates and, once close enough, by sight. Once a selected CAFO was identified by sight, the UWKA pilot would perform a visual safety inspection of the area and then fly up/down in a spiral pattern centered on the selected CAFO. The aircraft proceeded to circle the target CAFO at a low altitude to confirm in situ enhancements of CH<sub>4</sub> and NH<sub>3</sub> mixing ratios and the direction of the outflow plume. Flight altitudes ranged from 0.1 km AGL to 3 km AGL, and near-CAFO flight altitudes depended on safety constraints.

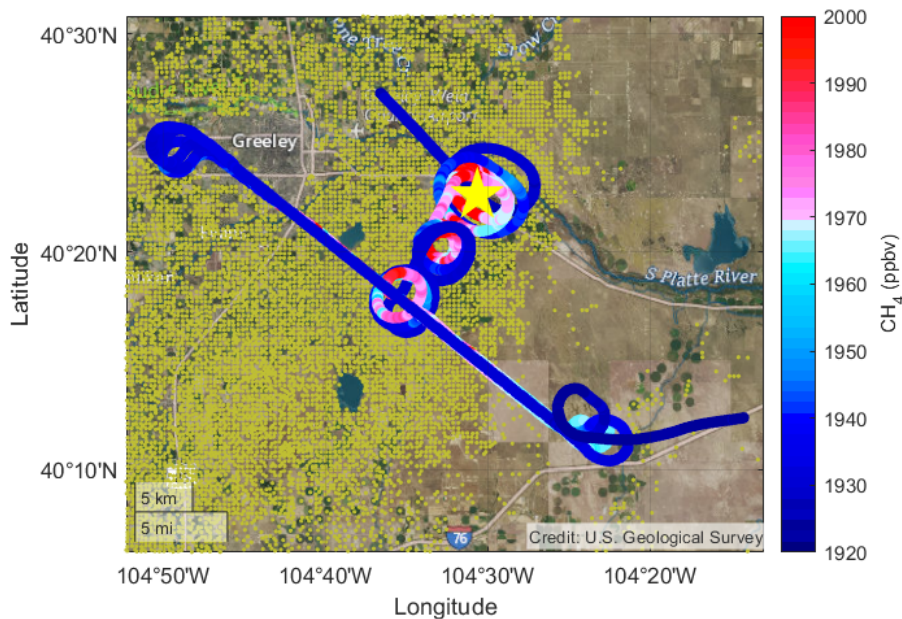


**Figure 2.** Observed CAFO (yellow star) flight path colored-filled with CH<sub>4</sub> (ppbv). Yellow dots represent ONG wells, data of ONG as of 2015 (Colorado Department of Natural Resources Oil & Gas Conservation Commission, 2016).

NH<sub>3</sub> deposition calculations are not the focus of this work, however, observations of deposition require multiple downwind observations. NH<sub>3</sub>:CH<sub>4</sub> ratios should be calculated near the source, as documented in Pollack et al. (2022) which used the same data set as this work. We investigated both spiral (which can be completed quickly) and horizontal transect flight patterns (which require much more flying time), shown in Fig. 2. The spiral patterns can be executed in quick succession, provide information as to the upwind background and provide multiple downwind distances for analysis of NH<sub>3</sub> deposition. However, the spiral transects were found to be undesirable for quantifying emissions because the aircraft could not get far enough outside the plume to characterize background conditions. For example, the further downwind spiral transects had high enhancements of CH<sub>4</sub> and NH<sub>3</sub> for the full width of the spiral, indicating that the UWKA did not leave the plume. The horizontal transects, while ideal for emission calculation, did not provide much information as to the evolution of downwind NH<sub>3</sub> deposition. In order to sample the full plume efficiently and provide multiple downwind observations, racetrack patterns or boxes were later identified as a preferred approach for future sampling.

### 2.3 Emission Calculations

CAFOs suited for emission calculations were identified based on the following requirements: (1) enhancements of CH<sub>4</sub> and NH<sub>3</sub> above background conditions, (2) flight path includes multiple transects downwind at different altitudes within the MBL, and (3) enough data near the target CAFO, but outside the CAFO plume, to characterize background mixing ratios. Only one CAFO sampled on November 13, 2019 satisfied the stated requirements to be suitable for emission quantification and is used



in the remainder of this work. The flight on November 13, 2019 (denoted as F2 from here forward) occurred during a period with strong and steady winds (average wind speed of  $8.4 \pm 2.7$  m/s) from the north-northeast (average wind direction  $32 \pm 0.65^\circ$ ). The MBL was well mixed with a top at  $1200 \pm 150$  m AGL (Fig. S1). The target CAFO, which holds a maximum capacity of 98,000 head of cattle, produced large enhancements of  $\text{CH}_4$  and  $\text{NH}_3$  at downwind distances of 1-14 km. The aircraft performed spiral transects at 4 km- 14 km downwind and stacked horizontal transects 12 km downwind. The CAFO sampled during F2 is surrounded by many ONG wells and is located 16 km southeast of Greeley, Colorado, an urban area with a population  $>100,000$ .

We used a mass-balance approach to calculate emissions. Aircraft mass-balance has been used to quantify emissions from a variety of source types (examples include Cambaliza et al. (2014); Caulton et al. (2014); Karion et al. (2015); Peischl et al. (2015, 2018)). Briefly, the mass flow rate of a species through a crosswind plane downwind of the source is approximated by the integration of enhancement above a background concentration over the width and height of the plume. The emissions are derived using Eq. 1 shown here:

$$M(u) = \int_0^{Z_{MBL}} \int_{-x}^x (C_u - C_b) \times U_{\perp} \times \rho(z) dx dz \quad (1)$$

In Eq. 1,  $M$  represents the molar flux ( $\text{moles s}^{-1}$ ) of a gas downwind of the source. To find the enhancement, the local background concentration,  $C_b$  (ppbv), is subtracted from the measured concentration,  $C_u$ . The ideal gas law is used to calculate the air density ( $\rho$ ) at every data point, using the universal gas constant at  $8.31 \text{ J mol}^{-1} \text{ K}^{-1}$ . The values  $\pm x$  are the horizontal limits of the plume width from the center point, and  $Z_{MBL}$  is the top of the MBL. The plume's height is projected to be from ground level to the top of the MBL. A vertical profile near the source was used to identify the MBL level using  $\text{H}_2\text{O}$  vapor and calculated potential temperature (Fig. S1). We used a constant value to represent the regional background. The background region was determined from the edges of the horizontal transects for the observed CAFO and used to calculate average values for  $\text{CH}_4$ ,  $\text{NH}_3$  and  $\text{C}_2\text{H}_6$ .

We transformed all observations surrounding the CAFO sampled during F2 (Fig. 2) onto a polar coordinate system ( $r, \theta$ ) using the center of the CAFO as the origin, following the process described in Nathan et al. (2015). The location of the data point on the polar coordinate system ( $\theta$ ) is perpendicular to the theoretical flux surface. So that,  $U_{\perp}$  ( $\text{m s}^{-1}$ ) is the corrected perpendicular wind by taking the cosine of the location of the data point on the polar coordinate system ( $\theta$ ) subtracted by wind direction ( $\phi$ ), multiplied by the wind magnitude ( $V$ ):

$$U_{\perp} = \cos(\theta - \phi) \times V \quad (2)$$

## 2.4 Uncertainty Analysis

We conducted an uncertainty analysis using a Monte Carlo approach, creating a pseudo distribution of the data and recalculating the emissions rates. Due to the nature of the plume, not all variables may be represented using a pseudo distribution. We define



the final emission uncertainty as the magnitude of the change in the emission from a combined function of the pseudo distributions of the following five parameters: background value, perpendicular wind speed, density, MBL depth, and instrumental uncertainty. The Monte Carlo recalculations were first done for individual parameters then as a combined pseudo distribution of perpendicular winds, density, background values, and MBL depth to calculate the final uncertainty. The uncertainty for the attribution methods followed the same approach but is addressed separately.

For the uncertainty analysis, we used a Gaussian distribution based on the mean and standard deviation of the original background value to select a new background value randomly. We found the density to have a pattern of increased values to one side of the horizontal transects. Therefore, to account for the pattern, we created a Gaussian distribution using the standard deviation found in each transect and added that onto a moving mean of 1 minute. The MBL height pseudo distribution was formed using a uniform randomly selected value of  $2600 \pm 150$  m AMSL. Throughout the day, the MBL height changed by an average of 150 m. The perpendicular winds consist of two variables: wind speed and wind direction. For each separate transect, we created a pseudo-Gaussian distribution of wind speed and wind direction based on the transects' mean and standard deviations for each variable. These Gaussian distributions of wind speed and direction were recalculated through Eq. 2 to produce the new perpendicular wind speeds. The emission recalculations were done 1000 times using all four parameters for  $\text{CH}_4$ ,  $\text{C}_2\text{H}_6$ , and  $\text{NH}_3$ . The uncertainty of final emission estimates were calculated by using the 95% confidence interval (CI) from the Monte Carlo approach divided by the average emission.

When considering the effect of instrumental uncertainty we only examine the factors actually impacting the measurements used in the mass-balance equation: the delta value ( $C_u - C_b$ ). Thus, even though we can report total instrumental uncertainty, this is not an appropriate metric to propagate through our uncertainty analysis. Total uncertainty values represent the best estimate of how the mixing ratio reported by the instrument compares to the actual value of the measured air mass. Such numbers include effects of instrument precision and accuracy, as well as uncertainty of calibration standards. However, an accurate measurement is actually not necessary to calculate emission rates (or any other quantity that relies on a delta value).

Instead of considering total uncertainty we consider what affects the uncertainty of the delta value. There are two factors: (1) the intercept (bias), and (2) the slope (calibration factor) of the instrument. The bias, which can be affected by drift in the zero reading, is quantified for  $\text{NH}_3$  and  $\text{C}_2\text{H}_6$ . To further clarify why these are the only instrumental uncertainty factors we evaluate and why total uncertainty does not affect our results we consider the following hypothetical situation: two otherwise identical instruments are used to quantify the same enhancement. One instrument reads a background value of  $1\text{E}6 \pm 0.1$  and peak value of  $1.000001\text{E}6$ . The second reads a background value of  $1 \pm 0.1$  and an enhancement of 2. The resulting delta values have the same absolute value and uncertainty because of how error propagates through subtraction regardless of which instrument was accurate. We assume that the variability in the bias is dwarfed by real variability in the background, or if the bias is actually large it similarly affects the background reading. Thus, we expect our analysis of background variability to be the appropriate metric to account for bias.

The uncertainty on the calibration factor is also possible to analyze and include. As far as we are aware, this source of uncertainty does not appear to be routinely reported or incorporated into uncertainty analysis in the mass balance literature. We assumed that the applied calibration factor can vary randomly and applied a randomly picked factor to the delta value to



create a pseudo distribution of possible enhancements. Note that the accuracy of the sensor doesn't matter. If uncertainty of the delta value is calculated in the fashion described, there would be equivalent uncertainty on an accurate or inaccurate reading provided the variability of the background and calibration factor was the same. This is not to argue for inaccurate sensors, but to explain why we have chosen to analyze uncertainty this way. The variability of the calibration factor was <0.1% for CH<sub>4</sub> and 9% for C<sub>2</sub>H<sub>6</sub>. For NH<sub>3</sub>, Pollack et al. (2019), found the variability to be 2%.

The effects of precision, which affect both background values and enhancements are neglected because we average a large area to calculate the background and bin average 5s of data for the enhancements. Averaging has the effect of decreasing the random error. The 1-Hz inflight precision is already low at 1 ppb for CH<sub>4</sub> (Picarro), 200 ppt for C<sub>2</sub>H<sub>6</sub>, and 60 ppt for NH<sub>3</sub> (Pollack et al., 2019). Comparatively, the observed variability in the background values dwarfs the error from precision at 33 ppbv, 3 ppbv and 4 ppbv for CH<sub>4</sub>, C<sub>2</sub>H<sub>6</sub> and NH<sub>3</sub>, respectively, thus we would expect the error introduced from precision to be negligible.

## 2.5 CH<sub>4</sub> Attribution

The two methods described here were applied to either all the data within the MBL during the flight (abbreviated F2), or only the downwind transects used for emission calculation (abbreviated Transect). This provides a total of four scenarios that will be analyzed. Ratios are reported in percentage (ratio x 100) across all methods.

### 2.5.1 Subtraction Method

The first attribution approach, referred to as the subtraction method (SM), removes the CH<sub>4</sub> emissions related to ONG and attributes the excess CH<sub>4</sub> emission to the CAFO. Rather than using inventory estimates for interfering sources, we calculated observation-based C<sub>2</sub>H<sub>6</sub>: CH<sub>4</sub> ratios. The F2 ratio (11 ± 0.02 %) is from Pollack et al. (2022). Briefly, NH<sub>3</sub> values >5 ppbv were used to screen out data points associated with CAFOs. The remaining data points were assumed to be associated with ONG sources, and the slope was calculated using least squares orthogonal distance regressions (ODR). The slope is equivalent to the C<sub>2</sub>H<sub>6</sub>: CH<sub>4</sub> enhancement ratio. Such a ratio can also be calculated from the CAFO transects as there was a region of CH<sub>4</sub> and C<sub>2</sub>H<sub>6</sub> signal that did not include NH<sub>3</sub> interference located on the northwest end of the transect. The resulting ratio for the Transect data following the identical calculation is 14.7 ± 0.6%. The ONG CH<sub>4</sub> emissions were removed through Eq. 3:

$$M_{CH_4_{ag}} = M_{CH_4} - CH_4 : C_2H_6 \times M_{C_2H_6} \quad (3)$$

The inverse of the C<sub>2</sub>H<sub>6</sub>: CH<sub>4</sub> ratio is used with the emission rate of C<sub>2</sub>H<sub>6</sub> (moles s<sup>-1</sup>) to retrieve the portion of CH<sub>4</sub> associated with ONG; that value is subtracted from the total CH<sub>4</sub> emission rate to result in the CH<sub>4</sub> emission associated with the CAFO. Finally, the molar emission rate (moles s<sup>-1</sup>) is multiplied by the molar mass to return the emission estimate in grams s<sup>-1</sup>.





## 2.5.2 Multivariate Regression

An alternative to the SM is to directly calculate the CAFO CH<sub>4</sub> emissions from an NH<sub>3</sub>: CH<sub>4</sub> ratio and the NH<sub>3</sub> emission rate using MVR. Because of the widespread ONG activity in this region, it is not always possible to have clear regions to calculate a ratio using a traditional regression approach (as in the SM). Indeed, there is also concern that the ratios calculated in the SM may not be accurate due to the influence of diffuse CAFO/agricultural signals. Fig. 3 presents C<sub>2</sub>H<sub>6</sub> and NH<sub>3</sub> mixing ratios plotted against CH<sub>4</sub>. In both plots there are elevated regions of the other species (i.e. regions of elevated C<sub>2</sub>H<sub>6</sub> in the NH<sub>3</sub> vs CH<sub>4</sub> plot). Instead, MVR using CH<sub>4</sub>, C<sub>2</sub>H<sub>6</sub>, and NH<sub>3</sub> data can be used to calculate NH<sub>3</sub>:CH<sub>4</sub> and C<sub>2</sub>H<sub>6</sub>:CH<sub>4</sub> ratios, as described in Pollack et al. (2022). Briefly, C<sub>2</sub>H<sub>6</sub> and NH<sub>3</sub> are assumed to be independent tracers (associated with ONG and the CAFO, respectively) and CH<sub>4</sub> is the dependent variable, as shown in Eq. 4. In this equation, *a* is the background CH<sub>4</sub> mixing ratio, *b* is the inverse effective NH<sub>3</sub>:CH<sub>4</sub> ratio and *c* is the inverse SM C<sub>2</sub>H<sub>6</sub>:CH<sub>4</sub> ratio. Unlike Kille et al. (2019) and Pollack et al. (2022), we did not subtract a background mixing ratios from the observed CH<sub>4</sub>, NH<sub>3</sub> or C<sub>2</sub>H<sub>6</sub> mixing ratios, thus the ‘*a*’ variable actually represents the local background and we can compare its value to the observed background we identified at the edges of the transect. Kille et al. (2019) performed sensitivity analysis on their MVR results. Following the guidance of Kille et al. (2019), we only use the MVR results when all three variables are positive, R<sup>2</sup> > 0.5 and all variables are statistically different from 0. We also tested scenarios with background subtracted CH<sub>4</sub>, NH<sub>3</sub> and C<sub>2</sub>H<sub>6</sub> to compare to the approaches used in Kille et al. (2019) and Pollack et al. (2022). We performed this analysis on the entire F2 dataset versus the Transect only data. The results of these sensitivity analyses are reported in Tables S1-2. The choice of background made no difference to the ratios, and only affected value *a*. This is consistent with Kille et al. (2019) and Pollack et al. (2022). Generally, scenarios where NH<sub>3</sub> and C<sub>2</sub>H<sub>6</sub> were not background subtracted produced ‘*a*’ values more consistent with the observed CH<sub>4</sub> background and were used for the remainder of the analysis. Slight differences in the MVR results were observed from Pollack et al. (2022). This is attributed to the differences in the area used for MVR between these studies; Pollack et al. (2022) isolated specific source regions for MVR analysis while this study uses all of the data in the study region.

$$CH_4 = a + b \times NH_3 + c \times C_2H_6 \quad (4)$$

## 3 Results & Discussions

### 3.1 CAFO Emissions

Fig. 4 shows curtain plots of the measured CH<sub>4</sub>, NH<sub>3</sub>, and C<sub>2</sub>H<sub>6</sub> mixing ratios from the horizontal transects. The curtain plots display the data from the flight paths in color-filled boxes representing the area used for the calculation in Eq. 1. In general, elevated NH<sub>3</sub> coincides with elevated CH<sub>4</sub>, indicating the presence of an agricultural plume. However, a high C<sub>2</sub>H<sub>6</sub> enhancement appears to be embedded in the agriculture plume, verifying mixed sources of CH<sub>4</sub> in this region. To isolate the agriculture plume and minimize the influence of other sources of CH<sub>4</sub>, we created a mask around the NH<sub>3</sub> signal and screened

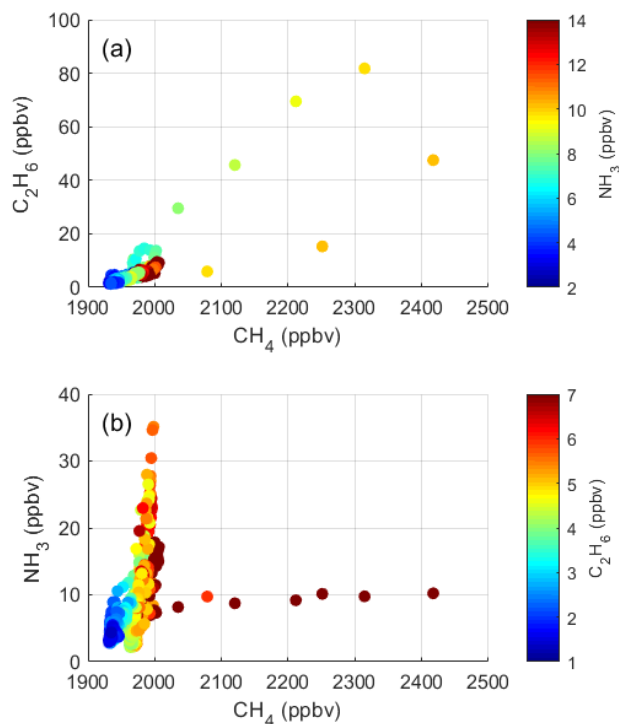


**Figure 3.** Scatter plots of (a)  $C_2H_6$  versus  $CH_4$  colored by the mixing ratio of  $NH_3$  and (b)  $NH_3$  versus  $CH_4$  colored by the  $C_2H_6$  mixing ratio sampled during the horizontal transects on 13 Nov 2019.

out points that were  $< 5$  ppbv of  $NH_3$  (Fig. 4e). This threshold was identified by Pollack et al. (2022), and was calculated as two times the maximum  $NH_3$  mixing ratio observed outside of the plumes of individual CAFOs and within the MBL. The resulting mask was used to limit the area integrated for emission estimates according to Eq. 1. The calculated emission rates are  $3330 \text{ g s}^{-1}$ ,  $609 \text{ g s}^{-1}$  and  $542 \text{ g s}^{-1}$  for  $CH_4$ ,  $NH_3$ , and  $C_2H_6$ , respectively.

250 We present an in-depth look at the uncertainty contributed by each parameter for  $CH_4$  emissions only. Perpendicular winds, density, and MBL depth are consistent in the calculations of  $NH_3$  and  $C_2H_6$  emissions; thus, we only discuss total uncertainty for these. Total uncertainty distribution plots are shown in Fig. S2.

Variability in density had little impact ( $< 1\%$ ) on the final  $CH_4$  emission rate. The winds during F2 had a standard deviation of  $\pm 2.7 \text{ m/s}$  with small changes in the wind direction with increased altitude. The recalculation of perpendicular wind speeds  
255 changed the final  $CH_4$  emissions by 4%. The location of the background in this study had a relatively consistent  $CH_4$  mixing ratio ( mean = 1933 ppbv, standard deviation = 1 ppbv). The background is similar to the regional background (1990 ppbv) identified by Pollack et al. (2022). Background variation affects the final  $CH_4$  emissions by 5%.  $NH_3$  had higher variations in background values leading to increased uncertainty overall. MBL height was the largest driver of uncertainty and was associated with an 8% change in  $CH_4$  emissions. The significant uncertainty due to MBL depth is expected; as changes in  
260 MBL depth would result in the interpolation of a different area without a response in concentration measurements. Thus, if the

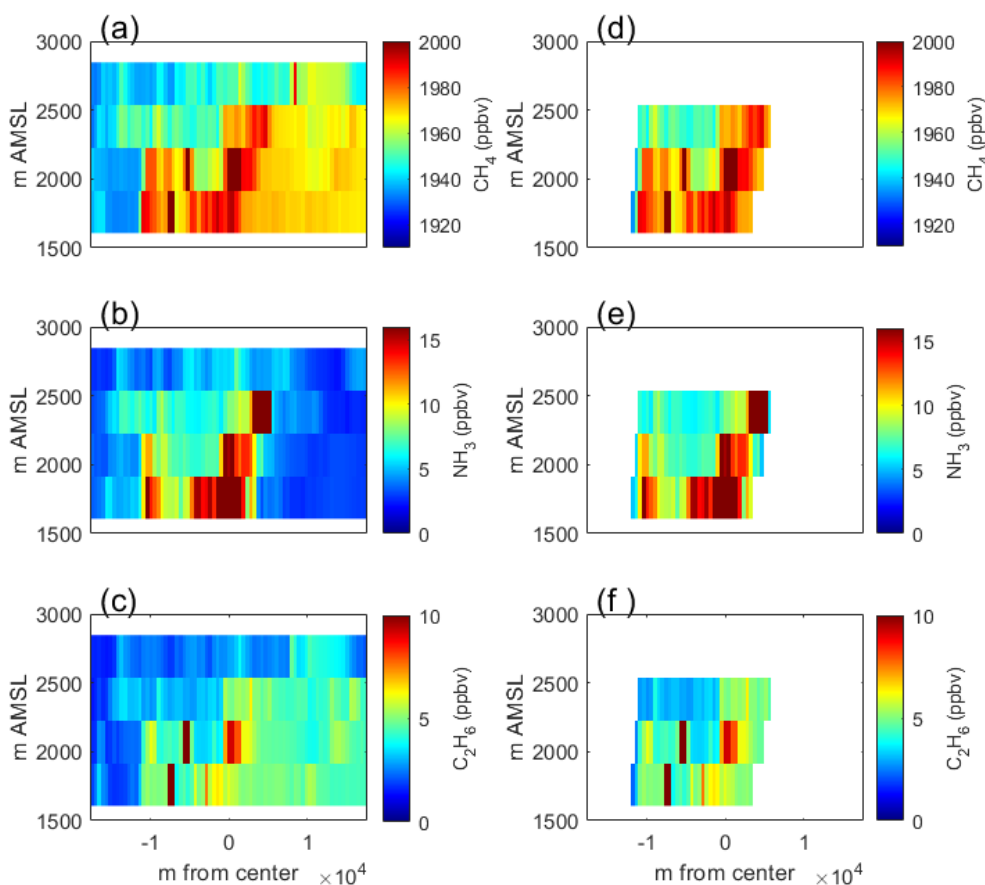


**Figure 4.** Vertical curtain plots of horizontal transects a) CH<sub>4</sub>, b) NH<sub>3</sub> and c) C<sub>2</sub>H<sub>6</sub> 12 km downwind of the observed CAFO. For reference, the surface is located at 1400 MSL. Vertical curtain plot of d) CH<sub>4</sub>, e) NH<sub>3</sub> and f) C<sub>2</sub>H<sub>6</sub> where NH<sub>3</sub> > 5 ppbv downwind of the observed CAFO.

MBL depth would have increased there is likely to be a corresponding decrease in concentrations. The absence of data between the lowest altitude transects and the surface may affect the accuracy of the results, but the associated uncertainty cannot be quantified because we do not have data at the surface. Instrumental uncertainty had little impact, changing the emission rates by <1% for all, CH<sub>4</sub> (0.3%), NH<sub>3</sub> (0.6 %), and C<sub>2</sub>H<sub>6</sub> (0.5%).

265 Cambaliza et al. (2014) carried out a detailed analysis on uncertainty from aircraft mass balance calculations. They found that MBL depth and background mixing ratios may have uncertainties up to 19% and 21%, respectively, on the overall emission rate estimate. Other studies have confirmed that uncertainty associated with the MBL depth makes a large contribution to overall uncertainty for these types of calculations (Karion et al., 2013; Peischl et al., 2015). The winds in the mass balance are assumed consistent from the release of the emissions to location of measurement. Therefore, the natural variability of winds



**Table 1.** CH<sub>4</sub> Attribution Sensitivity

Approach	Data	NH <sub>3</sub> :CH <sub>4</sub> (%) (SE) <sup>a</sup>	C <sub>2</sub> H <sub>6</sub> :CH <sub>4</sub> (%) (SE) <sup>a</sup>	CAFO CH <sub>4</sub> (g s <sup>-1</sup> ) (95% CI)	CAFO Relative Uncertainty (%)	n	Comments <sup>d</sup>
SM	F2	87 <sup>c</sup>	11 (0.02) <sup>c</sup>	697(±423)	61%	12,195 <sup>c</sup>	Fails criteria 1,2,3 & 4
SM	Transect	45	14.7 (0.7)	1,359 (±442)	34%	201	Fails criteria 1,2 & 3
MVR	F2	157 (2)	15.8 (0.1)	366 (±60)	17%	6,715	Fails criteria 1 & 2
MVR	Transect	92 (6)	17 (0.3)	626 (±122)	20%	1,568	Passes all criteria

<sup>a</sup> SE = standard error. <sup>b</sup> CI = confidence interval. <sup>c</sup> Pollack et al. (2022). <sup>d</sup> Criteria are defined in Sect. 3.2.

270 may contribute to the uncertainty more with less consistent winds (including direction and speed) and may have a large effect  
 on the final uncertainty similar to MBL and background value (Karion et al., 2013; Peischl et al., 2015). During F2 winds were  
 consistent and made a smaller contribution to the overall uncertainty.

The total uncertainty for CH<sub>4</sub> emissions calculated from horizontal transects was ± 10%. For the emissions estimates for  
 C<sub>2</sub>H<sub>6</sub> and NH<sub>3</sub>, the total uncertainty was ± 14% and ± 17%, respectively. Other factors that may influence the accuracy of  
 275 the emissions include smaller-scale variations in the mixing ratios and regions of the plume the flights did not sample. As it is  
 not possible to sample the entire MBL from top to bottom, the vertical spacing between the horizontal transects may result in  
 errors. Errors associated with interpolation were not explored here, but are expected to be small (Cambaliza et al., 2014). The  
 uncertainty estimates are specific to this flight. Different meteorological conditions can produce different uncertainty estimates.  
 In particular, MBL uncertainty or growth may significantly affect the magnitude of the uncertainty. The uncertainty analysis  
 280 methodology presented here can be applied to any future mass-balance emission estimates.

### 3.2 CAFO CH<sub>4</sub> Attribution: Comparison of Methods

Results from the SM and MVR CAFO CH<sub>4</sub> attribution and associated uncertainty are presented in Table 1. Reported uncer-  
 tainties in Table 1 represent results from combining the ratio uncertainty to the rest of the pseudo distributions as described  
 in Sect. 2.4. Both the magnitude of the attributed CAFO CH<sub>4</sub> emission and its uncertainty vary between approaches. These  
 285 methods represent typical approaches that can be undertaken to isolate the emissions for a given facility. In order to identify  
 the optimal method, we identify four criteria: (1) the relationships should predict the total CH<sub>4</sub> well; in other words traditional  
 goodness of fit (GOF) values should be optimal (the average residual of the fit should be near 0 and R<sup>2</sup> values should be high),  
 (2) the relationships for NH<sub>3</sub>:CH<sub>4</sub> and C<sub>2</sub>H<sub>6</sub>:CH<sub>4</sub> should be consistent with observations, (3) the method should err on the side  
 of being conservative, meaning it should be more likely to under-attribute than over-attribute the CAFO emissions, and (4)  
 290 uncertainty of the result should be low. As currently presented these criteria are qualitative, because each analysis is unique.  
 We will discuss the implications and further refinements of these criteria later on. These criteria are presented in order of their  
 importance to the final recommendation. This approach ensures that low uncertainty is not the primary deciding factor.



To investigate criteria 1, we calculated total fits, residuals and  $R^2$  values for all four methods and assessed how well the  $\text{NH}_3:\text{CH}_4$  and  $\text{C}_2\text{H}_6:\text{CH}_4$  ratios represented the transect data. The central assumption is that regardless of attribution method, all methods should predict the observed  $\text{CH}_4$  values well as evaluated by traditional metrics of goodness of fit (e.g.  $R^2$ , residuals). MVR directly produces both ratios such that predicted  $\text{CH}_4$  can be calculated from the  $\text{NH}_3$  and  $\text{C}_2\text{H}_6$  time series. To construct a  $\text{CH}_4$  prediction for the SM, which does not require calculation of  $\text{NH}_3:\text{CH}_4$  ratios, we inferred the effective  $\text{NH}_3:\text{CH}_4$  ratio from the ratio of the calculated  $\text{NH}_3$  emissions to the  $\text{CH}_4$  attributed to the CAFO by SM. The resulting ratio is then used in Eq. 4 to produce an effective multivariate regression prediction. Table S3 shows the full range of variables for each scenario. GOF statistics are calculated for the transect data only.

The results of this comparison are shown in Fig. 5, with the prediction limited to the Transect data, because this is the data that is actually used to calculate the  $\text{CH}_4$  emission rate. The Transect MVR approach was the method with the best GOF statistics including an average residual closest to 0 and the highest  $R^2$  value and the only approach that passes criteria 1. In some ways this is unsurprising because fits are calculated by minimizing the sum of the residual squared, and this is the only method that directly fits the Transect data (Skoog et al., 2004). Still, this analysis does provide the means to compare the other methods and can be useful when site specific MVR is not possible. The background values were consistent in all methods and consistent with observations. The three other methods all overpredicted  $\text{CH}_4$  and had average negative residuals and lower  $R^2$  values. The over-prediction suggests that these methods produce an incorrect relationship between  $\text{CH}_4$  and one (or both) of the tracer gases, but it is not possible to identify which relationship is incorrect. The method that best simulates the data after the Transect MVR is the F2 MVR.

The effective  $\text{NH}_3:\text{CH}_4$  ratios produced for this method can also be compared directly in support of criteria 2. Criteria 2 is difficult to evaluate because ideally the actual ratios would be known. We can compare to literature values, compare values between scenarios, and look at the underlying assumptions of the calculations to evaluate this criteria. The  $\text{C}_2\text{H}_6:\text{CH}_4$  ratios calculated for SM and MVR varied by 40%, which substantially affects how much  $\text{CH}_4$  is attributed to ONG. However, the range of ONG ratios is broadly consistent with other observations in this region (Kille et al., 2017, 2019; Yacovitch et al., 2017; Peischl et al., 2018).

As a plume moves downwind from its source it is expected that the plume will disperse over the MBL.  $\text{NH}_3$  has a short lifetime and may be removed through dry deposition and transition into the particle phase. Thus, there may be lower concentrations downwind of gaseous  $\text{NH}_3$  than expected from dilution alone. Pollack et al. (2022) show that the transects located 12 km downwind of the observed CAFO do not have the same  $\text{NH}_3:\text{CH}_4$  ratio as plume transects collected closer to the CAFO. There is also generally a wide variety of ratios reported in Pollack et al. (2022) ranging from 80% to 270% across different facilities which illustrates why the MVR results from the full F2 data may not be appropriate to represent an individual site. In general, the SM produced ratios that were lower than MVR and observations near the source (Pollack et al., 2022). The SM Transect ratio is particularly low (45%), about half the value of any other ratio produced from the other attribution methods. This indicates that this approach actually fails criteria 2.

On a theoretical basis, the MVR ratios calculated from the F2 data include locations near other CAFOs and locations near ONG sources. Therefore, the F2 MVR results may not accurately represent the area around this particular CAFO. The SM using

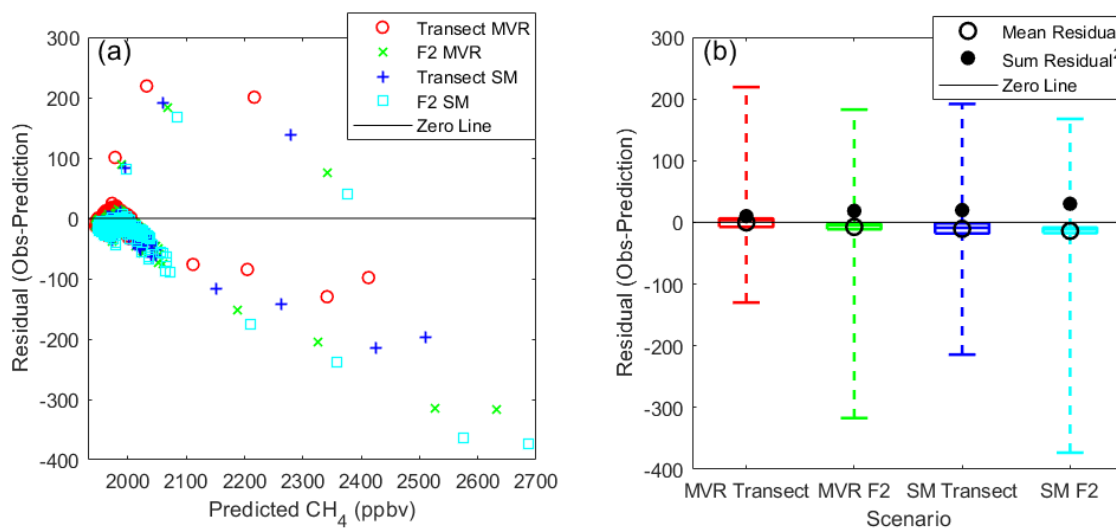


**Figure 5.** a) Residual  $\text{CH}_4$  (observation - prediction) vs. predicted  $\text{CH}_4$  (ppbv). The ratios corresponding to the transect MVR results are shown in red, the F2 MVR results are shown in green, the transect SM results are shown in blue, and the F2 SM results are shown in cyan. The black line in both plots represents the zero line. b) Box plots of residuals for the four different methods. Residual boxplot of the different methods. The central line in each box represents the median, the box shows the 25-75% quartile range, and the capped dashed lines show the full data extent (no data are excluded as outliers). The open black dots are the calculated mean residual and the closed black dots are the sum of the residuals squared (normalized by the minimum value  $\times 10$ ). The boxplot is ordered by increasing absolute average residual.

F2 data has similar challenges. The SM assumes that  $\text{C}_2\text{H}_6:\text{CH}_4$  is constant throughout the area and that there are no other sources of  $\text{CH}_4$  other than the CAFO and ONG. However, we know there may be other trace amounts of  $\text{CH}_4$  from vehicles, waste areas, and other small sources. Generally, we would expect data nearest the source to produce the most accurate ratios and pass criteria 2. This would generally exclude the F2 results and for this reason, we assume these results fail criteria 2.

For criteria 3, the two methods are different in approach and it is quite easy to identify which approach is more conservative. The SM attributes anything outside of ONG to the CAFO plume, thus there is no unattributed  $\text{CH}_4$  for these methods. The SM is, therefore, expected to be less conservative and an upper limit of the CAFO  $\text{CH}_4$  emissions due to the possibility of other sources in the region.

In the MVR approach, the  $R^2$  value of the fit gives an estimate of how much of the  $\text{CH}_4$  signal is explained by the chosen tracers. The MVR fits had  $R^2$  values of 0.72 for F2 and 0.74 for Transects, which leaves an amount of  $\text{CH}_4$  that is not well correlated to  $\text{NH}_3$  or  $\text{C}_2\text{H}_6$ . In this scenario, this excess  $\text{CH}_4$  is left unattributed in the MVR approach (56% for F2 and 24% for Transect). A visual representation of the unattributed portion of the  $\text{CH}_4$  signal for the transect MVR is presented in Fig. S3. The unattributed  $\text{CH}_4$  is broadly distributed and cannot be attributed to any particular source. The MVR approach avoids over-attributing the  $\text{CH}_4$  signal to the CAFO.



In general, we expect the Transect MVR approach which uses the data closest to the source to provide the best estimate of this CAFOs emissions in accord with the first three criteria. This approach produces local ratios on par with the literature, has the closest average residual to 0 and is conservative in its approach to attribution. This is, however, not the result with the lowest uncertainty. Both the MVR results have lower uncertainty than SM because they do not require subtraction. The impact of subtraction on uncertainty is evident in Table 1 and is the basis for including criteria 4. While the ONG ratios calculated either by SM or MVR using the F2 data differ by 40%, the uncertainty on the results using MVR attribution is a factor of 3 lower. This is despite the fact that the SM ratio uncertainty is actually a factor of 5 lower than the MVR ratio. If we had used a comparable error on the  $C_2H_6:CH_4$  ratio to MVR with SM, the error would approach 100%. The primary reason for the difference in uncertainty between the SM and MVR approaches relates to how error is propagated through subtraction vs. multiplication or division. For subtraction, absolute errors add in quadrature, while for multiplication/division, relative errors add in quadrature (Skoog et al., 2004). The net effect is that error on the SM will be very high when the absolute amount to be subtracted is large. The ONG ratio is not directly used for attribution in the MVR approach, which is why the CAFO attributed emissions by the F2 MVR and SM approaches vary by 30%. However, the relative uncertainty (standard error/ratio) on the  $NH_3:CH_4$  MVR ratio is comparable to the relative uncertainty of the MVR ONG ratio.

The subtraction method is very similar to inventory subtraction in principle. Error estimates are often not provided for inventory data, but the error introduced to emission estimates by subtracting inventories may be substantial. Zimmerle et al. (2022) recently showed how ONG sources could vary and produce uncertainties in excess of estimates relying on traditional inventory data. The MVR approach is generally attractive to avoid such errors when interfering signals are high and there is enough data to produce robust MVR results. The plume from the observed CAFO was broad, allowing for multiple data points within the plume and produced results with low uncertainty (20 %). For sites with narrower and lower enhancements local MVR may not be possible. Our criteria would suggest that using MVR on the full flight data may be an appropriate proxy when local ratios with MVR cannot be calculated. However, the results from the MVR Transect and F2 data are statistically different in this case. Additional analysis may need to be done to ensure the MVR results from larger data sets are applicable to the site of interest. Repeat measurements or ground observations would help to constrain such results.

### 3.3 Comparison to literature

A few recent studies have reported  $CH_4$  emission rates from CAFOs. The emissions factors calculated from the Transect MVR method in this work are  $23 (\pm 5) \text{ g } CH_4 \text{ head}^{-1} \text{ hr}^{-1}$  and  $22 (\pm 4) \text{ g } NH_3 \text{ head}^{-1} \text{ hr}^{-1}$ . The calculation of emission rates as a value per head is based on the maximum amount of cattle allowed in the CAFO, although the actual number of cattle in the CAFO at the time of the measurement is unknown. We found significantly higher emissions rates of both  $CH_4$  than many other beef cattle studies. The EPA estimated  $CH_4$  emissions for beef cattle is  $7.2 \text{ g head}^{-1} \text{ hr}^{-1}$  and previous studies range from 7 - 9 (EPA Annex, 2021; Golston et al., 2020; Hacker et al., 2016). Dairy cattle have high rates of  $CH_4$  emissions due to higher exertion on the animal with rates ranging from 14 - 39  $\text{g head}^{-1} \text{ hr}^{-1}$  and the EPA national average is  $18 \text{ g head}^{-1} \text{ hr}^{-1}$  (EPA Annex, 2021; Leytem et al., 2011; Bjerneberg et al., 2009; Griffith et al., 2008). Golston et al. (2020) conducted a ground-based study in NCFR and found the highest emission rates in dairy cattle at  $39.32 \pm 3.92 \text{ g } CH_4 \text{ head}^{-1} \text{ hr}^{-1}$ . In contrast, their reported



emissions from beef cattle were much lower and similar to other studies ( $9.48 \pm 0.93$  g CH<sub>4</sub> head<sup>-1</sup> hr<sup>-1</sup>). However, they noted there was a significant difference in emissions rates of repeat observation for an individual CAFO.

A large difference between the CH<sub>4</sub> emissions per head of cattle in this work compared to prior works could be due to the management of the CAFO. Enteric fermentation can be altered through the composition of the food given to the animals. 380 For instance, the type and maturity of diets provided to the animals may modify the nutrients and digestibility of the food (Archimède et al., 2011). CH<sub>4</sub> emissions from cattle are also known to depend on exertion on the animals including exercise and stress (EPA, 2022). In this study, the food source and feeding schedule were unknown. We also note that this CAFO was extremely large, one of the largest in Colorado, and most emissions estimates are based on considerably smaller CAFOs.

The NH<sub>3</sub> emissions per head reported here are also much higher than previous estimates, which ranged from 2-12 head<sup>-1</sup> 385 hr<sup>-1</sup> (Staebler et al., 2009; Golston et al., 2020; Hacker et al., 2016). The NH<sub>3</sub> emission per head calculation in our work does not require removal of interfering signals like the CH<sub>4</sub> emissions. The NH<sub>3</sub> are highly affected by meteorological conditions including seasonality and time of day. Waste that is stored outside may exacerbate NH<sub>3</sub> emissions in warmer temperatures (Montes et al., 2013). There is also evidence of a diurnal pattern of NH<sub>3</sub> emissions from CAFOs with a peak during noon local time, near the time of sampling in this work (Shonkwiler and Ham, 2017). NH<sub>3</sub>:CH<sub>4</sub> ratios follow a similar pattern with higher 390 ratios during the midday and lower ratios at night (Eilerman et al., 2016).

#### 4 Conclusions

We demonstrate an approach to isolate and quantify CH<sub>4</sub> plumes of agriculture CAFO sources with interfering sources by using SM and MVR methods. The SM method uses NH<sub>3</sub> as a tracer to identify a CAFO plume before using a C<sub>2</sub>H<sub>6</sub>:CH<sub>4</sub> ratio to remove any ONG CH<sub>4</sub> emissions interfering with the CAFO source. It is an optimal method when there is little ONG 395 influence to keep the error introduced from subtraction small. The MVR method uses C<sub>2</sub>H<sub>6</sub> and NH<sub>3</sub> as tracers and provides lower uncertainty on emission estimates. This approach is appropriate when tracer data is available and there is enough signal to produce statistically significant relationships and thus site specific ratios. The criteria to identify the best approach may be useful for isolating and attributing emissions from specific sources in other regions. Overall, our best estimates of emissions from the observed CAFO are  $23 (\pm 5)$  g hr<sup>-1</sup> head<sup>-1</sup> for CH<sub>4</sub> and  $22 (\pm 4)$  g hr<sup>-1</sup> head<sup>-1</sup> for NH<sub>3</sub>. These findings are significantly 400 higher than EPA inventory estimates and previous studies highlighting the need for more observations and estimates of CAFO CH<sub>4</sub> and NH<sub>3</sub> emission rates.

*Data availability.* Merged data files for the F2 data will be made available from WyoScholar <https://wyo scholar.uwyo.edu/> This long-term repository is open-access and provides freely available data stewarded by the University of Wyoming Libraries.

*Author contributions.* CRediT: <https://authorservices.wiley.com/author-resources/Journal-Authors/open-access/credit.html>





- 405 MEM: Writing-Original Draft, Formal Analysis, Visualization, Data Collection  
IBP: Writing-Review & Editing, Funding Acquisition, Data Collection  
EVF: Writing-Review & Editing, Funding Acquisition  
DRC: Conceptualization, Supervision, Writing-Review & Editing, Funding Acquisition, Data Collection

*Competing interests.* The authors declare no competing financial interests.

- 410 *Acknowledgements.* We would like to thank the University of Wyoming King Air facility for their support of this project. We would also like to thank Kristen Pozsonyi for help with instrument installation and data collection. This work was partly supported by the Transport and Transformation of Ammonia (TRANS2AM) Campaign funded by the National Science Foundation (grant #2020151).



## References

- Archimède, H., Eugène, M., Marie Magdeleine, C., Boval, M., Martin, C., Morgavi, D. P., Lecomte, P., and Doreau, M.:  
415 Comparison of methane production between C3 and C4 grasses and legumes, *Anim Feed Sci Tech*, 166-167, 59–64,  
<https://doi.org/10.1016/j.anifeedsci.2011.04.003>, 2011.
- Arnold, S., Dileo, J., and Takushi, T.: Colorado Greenhouse Gas Inventory — 2014 Update Including Projections to 2020 & 2030, Department  
of Public Health & Environment, 2014.
- Bjorneberg, D. L., Leytem, A. B., Westermann, D. T., Griffiths, P. R., Shao, L., and Pollard, M. J.: Measurement of Atmospheric Ammo-  
420 nia, Methane, and Nitrous Oxide at a Concentrated Dairy Production Facility in Southern Idaho Using Open-Path FTIR Spectrometry,  
*Transactions of the ASABE*, 52, 1749–1756, 2009.
- Cambaliza, M. O., Shepson, P. B., Caulton, D. R., Stirm, B., Samarov, D., Gurney, K. R., Turnbull, J., Davis, K. J., Possolo, A., Karion, A.,  
Sweeney, C., Moser, B., Hendricks, A., Lauvaux, T., Mays, K., Whetstone, J., Huang, J., Razlivanov, I., Miles, N. L., and Richardson,  
S. J.: Assessment of uncertainties of an aircraft-based mass balance approach for quantifying urban greenhouse gas emissions, *Atmos.*  
425 *Chem. Phys.*, 14, 9029–9050, <https://doi.org/10.5194/acp-14-9029-2014>, 2014.
- Caulton, D. R., Shepson, P. B., Santoro, R. L., Sparks, J. P., Howarth, R. W., Ingraffea, A. R., Cambaliza, M. O., Sweeney, C., Karion,  
A., Davis, K. J., Stirm, B. H., Montzka, S. A., and Miller, B. R.: Toward a better understanding and quantification of methane emis-  
sions from shale gas development, *Proceedings of the National Academy of Sciences of the United States of America*, 111, 6237–6242,  
<https://doi.org/10.1073/pnas.1316546111>, 2014.
- 430 CDPHE: Colorado Department of Public Health and Environment CAFO Permit Database, [www.colorado.gov/pacific/cdphe/  
animal-and-livestock-feeding-operations](http://www.colorado.gov/pacific/cdphe/animal-and-livestock-feeding-operations), accessed: Jan 27, 2021, 2017.
- Colorado Department of Natural Resources Oil & Gas Conservation Commission: Colorado Oil and Gas Information System (COGIS),  
[www.colorado.gov/pacific/cdphe/animal-and-livestock-feeding-operations](http://www.colorado.gov/pacific/cdphe/animal-and-livestock-feeding-operations), accessed: April, 2016, 2016.
- Crosson, E. R.: A cavity ring-down analyzer for measuring atmospheric levels of methane, carbon dioxide, and water vapor, *Appl. Phys.*  
435 *B-Lasers O*, 92, 403–408, <https://doi.org/10.1007/s00340-008-3135-y>, 2008.
- Eilerman, S. J., Peischl, J., Neuman, J. A., Ryerson, T. B., Aikin, K. C., Holloway, M. W., Zondlo, M. A., Golston, L. M., Pan, D., Floer-  
cheringer, C., and Herndon, S.: Characterization of Ammonia, Methane, and Nitrous Oxide Emissions from Concentrated Animal Feeding  
Operations in Northeastern Colorado, *Environ. Sci. Technol.*, 50, 10 885–10 893, <https://doi.org/10.1021/acs.est.6b02851>, 2016.
- EPA: Inventory of U.S. Greenhouse Gas Emissions and Sinks: 1990-2020. U.S. Environmental Protection Agency, Epa 430-R-18-003, pp.  
440 1–205, 2022.
- EPA Annex: U.S. Green House Gas Emissions and Sinks 1990-2019 Annex 3 Part B, 4, 1–71, <http://marefateadyan.nashriyat.ir/node/150>,  
2021.
- Golston, L. M., Pan, D., Sun, K., Tao, L., Zondlo, M. A., Eilerman, S. J., Peischl, J., Neuman, J. A., and Floercherger, C.: Variability of  
Ammonia and Methane Emissions from Animal Feeding Operations in Northeastern Colorado, *Environ. Sci. Technol.*, 54, 11 015–11 024,  
445 <https://doi.org/10.1021/acs.est.0c00301>, 2020.
- Griffith, D. W., Bryant, G. R., Hsu, D., and Reisinger, A. R.: Methane emissions from free-ranging cattle: Comparison of tracer and integrated  
horizontal flux techniques, *Aust. J. Exp. Agr.*, 48, 582–591, <https://doi.org/10.2134/jeq2006.0426>, 2008.



- Hacker, J. M., Chen, D., Bai, M., Ewenz, C., Junkermann, W., Lieff, W., McManus, B., Neining, B., Sun, J., Coates, T., Denmead, T., Flesch, T., McGinn, S., and Hill, J.: Using airborne technology to quantify and apportion emissions of CH<sub>4</sub> and NH<sub>3</sub> from feedlots, *Anim. Prod. Sci.*, 56, 190–203, <https://doi.org/10.1071/AN15513>, 2016.
- Higley, B. D. K. and Cox, D. O.: Oil and Gas Exploration and Development along the Front Range in the Denver Basin of Colorado, Nebraska, and Wyoming, USGS Province 39: U.S. Geological Survey Digital Data Series, Ch. 2, <http://www.usgs.gov/pubprod>, 2007.
- Karion, A., Sweeney, C., Pétron, G., Frost, G., Michael Hardesty, R., Kofler, J., Miller, B. R., Newberger, T., Wolter, S., Banta, R., Brewer, A., Dlugokencky, E., Lang, P., Montzka, S. A., Schnell, R., Tans, P., Trainer, M., Zamora, R., and Conley, S.: Methane emissions estimate from airborne measurements over a western United States natural gas field, *Geophys. Res. Lett.*, 40, 4393–4397, <https://doi.org/10.1002/grl.50811>, 2013.
- Karion, A., Sweeney, C., Kort, E. A., Shepson, P. B., Brewer, A., Cambaliza, M., Conley, S. A., Davis, K., Deng, A., Hardesty, M., Herndon, S. C., Lauvaux, T., Lavoie, T., Lyon, D., Newberger, T., Pétron, G., Rella, C., Smith, M., Wolter, S., Yacovitch, T. I., and Tans, P.: Aircraft-Based Estimate of Total Methane Emissions from the Barnett Shale Region, *Environ. Sci. Technol.*, 49, 8124–8131, <https://doi.org/10.1021/acs.est.5b00217>, 2015.
- Kille, N., Baidar, S., Handley, P., Ortega, I., Sinreich, R., and Cooper, O. R.: The CU mobile Solar Occultation Flux instrument: structure functions and emission rates of NH<sub>3</sub>, NO<sub>2</sub> and C<sub>2</sub>H<sub>6</sub>, *Atmos. Meas. Tech.*, 10, 373–392, <https://doi.org/10.5194/amt-10-373-2017>, 2017.
- Kille, N., Chiu, R., Frey, M., Hase, F., Sha, M. K., Blumenstock, T., Hannigan, J. W., Orphal, J., Bon, D., and Volkamer, R.: Separation of Methane Emissions From Agricultural and Natural Gas Sources in the Colorado Front Range, *Geophys. Res. Lett.*, 46, 3990–3998, <https://doi.org/10.1029/2019GL082132>, 2019.
- Leytem, A. B., Dungan, R. S., Bjorneberg, D. L., and Koehn, A. C.: Emissions of Ammonia, Methane, Carbon Dioxide, and Nitrous Oxide from Dairy Cattle Housing and Manure Management Systems, *J. Environ. Qual.*, 40, 1383–1394, <https://doi.org/10.2134/jeq2009.0515>, 2011.
- Maasackers, J. D., Jacob, D. J., Sulprizio, M. P., Turner, A. J., Weitz, M., Wirth, T., Hight, C., DeFigueiredo, M., Desai, M., Schmeltz, R., Hockstad, L., Bloom, A. A., Bowman, K. W., Jeong, S., and Fischer, M. L.: Gridded National Inventory of U.S. Methane Emissions, *Environ. Sci. Technol.*, 50, 13 123–13 133, <https://doi.org/10.1021/acs.est.6b02878>, 2016.
- Mielke-Maday, I., Schwietzke, S., Yacovitch, T. I., Miller, B., Conley, S., Kofler, J., Handley, P., Thorley, E., Herndon, S. C., Hall, B., Dlugokencky, E., Lang, P., Wolter, S., Moglia, E., Crotwell, M., Crotwell, A., Rhodes, M., Kitzis, D., Vaughn, T., Bell, C., Zimmerle, D., Schnell, R., and Pétron, G.: Methane source attribution in a U.S. dry gas basin using spatial patterns of ground and airborne ethane and methane measurements, *Elementa: Science of the Anthropocene*, 7, <https://doi.org/10.1525/elementa.351>, 13, 2019.
- Montes, F., Meinen, R., Dell, C., Rotz, A., Hristov, A. N., Oh, J., Waghorn, G., Gerber, P. J., Henderson, B., Makkar, H. P., and Dijkstra, J.: SPECIAL TOPICS-Mitigation of methane and nitrous oxide emissions from animal operations: II. A review of manure management mitigation options, *J. Anim. Sci.*, 91, 5070–5094, <https://doi.org/10.2527/jas.2013-6584>, 2013.
- Moumen, A., Azizi, G., Chekroun, B., and Baghour, M.: The effects of livestock methane emission on the global warming: A review, *Int. J. Global Warming*, 9, 229–253, <https://doi.org/10.1504/IJGW.2016.074956>, 2016.
- Myhre, G., Shindell, D., Bréon, F.-M. F.-M., Collins, W., Fuglestedt, J., Huang, J., Koch, D., Lamarque, J.-F. J.-F., Lee, D., Mendoza, B., Nakajima, T., Robock, A., Stephens, G., Takemura, T., Zhan, H., and Zhang, H.: Anthropogenic and Natural Radiative Forcing: Supplementary Material, *Climate Change 2013: The Physical Science Basis. Contribution of Working Group I to the Fifth Assessment Report of the Intergovernmental Panel on Climate Change: The Physical Science Basis. Contribution of Working Group I to the Fifth*



- 485 Assessment Report of the Intergovernmental Panel on Climate Change [Stocker, T.F., D. Qin, G.-K. Plattner, M. Tignor, S.K. Allen, J. Boschung, A. Nauels, Y. Xia, V. Bex and P.M. Midgley (eds.)], pp. 1–44, [www.climatechange2013.org](http://www.climatechange2013.org), 2013.
- Nathan, B. J., Golston, L. M., Brien, A. S. O., Ross, K., Harrison, W. A., Tao, L., Lary, D. J., Johnson, D. R., Covington, A. N., Clark, N. N., and Zondlo, M. A.: Near-Field Characterization of Methane Emission Variability from a Compressor Station Using a Model Aircraft, *Environ. Sci. Technol.*, <https://doi.org/10.1021/acs.est.5b00705>, 2015.
- 490 Peischl, J., Ryerson, T. B., Aikin, K. C., Gouw, J. A., Gilman, J. B., Holloway, J. S., Lerner, B. M., Nadkarni, R., Neuman, J. A., Nowak, J. B., Trainer, M., Warneke, C., and Parrish, D. D.: J. Geophys. Res. : Atmospheres Quantifying atmospheric methane emissions from the, *J. Geophys. Res.*, 120(5), 2119–2139, <https://doi.org/10.1002/2014JD022697>.Received, 2015.
- Peischl, J., Eilerman, S. J., Neuman, J. A., Aikin, K. C., de Gouw, J., Gilman, J. B., Herndon, S. C., Nadkarni, R., Trainer, M., Warneke, C., and Ryerson, T. B.: Quantifying Methane and Ethane Emissions to the Atmosphere From Central and Western U.S. Oil and Natural Gas  
495 Production Regions, *J. Geophys. Res.: Atmospheres*, 123, 7725–7740, <https://doi.org/10.1029/2018JD028622>, 2018.
- Picarro: G2401 Analyzer Datasheet, pp. 1–2, [https://www.picarro.com/support/library/documents/g2401\\_analyzer\\_datasheet](https://www.picarro.com/support/library/documents/g2401_analyzer_datasheet).
- Pollack, I. B., Lindaas, J., Robert Roscioli, J., Agnese, M., Permar, W., Hu, L., and Fischer, E. V.: Evaluation of ambient ammonia measurements from a research aircraft using a closed-path QC-TILDAS operated with active continuous passivation, *Atmos. Meas. Tech.*, 12, 3717–3742, <https://doi.org/10.5194/amt-12-3717-2019>, 2019.
- 500 Pollack, I. B., McCabe, M. E., Caulton, D. R., and Fischer, E. V.: Enhancements in Ammonia and Methane from Agricultural Sources in the Northeastern Colorado Front Range Using Observations from a Small Research Aircraft, *Environ. Sci. Technol.*, 56, 2236–2247, <https://doi.org/10.1021/acs.est.1c07382>, 2022.
- Richardson, S. J., Miles, N. L., Davis, K. J., Crosson, E. R., Rella, C. W., and Andrews, A. E.: Field testing of cavity ring-down spectroscopy analyzers measuring carbon dioxide and water vapor, *J. Atmos. Ocean Tech.*, 29, 397–406, <https://doi.org/10.1175/JTECH-D-11-00063.1>,  
505 2012.
- Roscioli, J. R., Zahniser, M. S., Nelson, D. D., Herndon, S. C., and Kolb, C. E.: New Approaches to Measuring Sticky Molecules: Improvement of Instrumental Response Times Using Active Passivation, *J. Phys. Chem. A*, 120, 1347–1357, <https://doi.org/10.1021/acs.jpca.5b04395>, 2015.
- Shonkwiler, K. B. and Ham, J. M.: Agr. Forest Meteorol. Ammonia emissions from a beef feedlot : Comparison of inverse modeling techniques using long-path and point measurements of fenceline NH<sub>3</sub>, *Agr. Forest Meteorol.*, 258, 29–42, <https://doi.org/10.1016/j.agrformet.2017.10.031>, 2017.
- Skoog, D. A., West, D. M., Holler, F. J., and Crouch, S. R.: *Fundamentals of Analytical Chemistry*, Thomson-Brooks/Cole, 8th edn., 2004.
- Smith, C., Nicholls, Z., Armour, K., Collins, W., Forster, P., Meinshausen, M., Palmer, M., and Watanabe, M.: *The Earth’s Energy Budget, Climate Feedbacks, and Climate Sensitivity Supplementary Material*, Available from <https://www.ipcc.ch/>, 2021.
- 515 Smith, M. L., Kort, E. A., Karion, A., Sweeney, C., Herndon, S. C., and Yacovitch, T. I.: Airborne Ethane Observations in the Barnett Shale: Quantification of Ethane Flux and Attribution of Methane Emissions, *Environ. Sci. Technol.*, 49, 8158–8166, <https://doi.org/10.1021/acs.est.5b00219>, 2015.
- Staebler, R. M., McGinn, S. M., Crenna, B. P., Flesch, T. K., Hayden, K. L., and Li, S. M.: Three-dimensional characterization of the ammonia plume from a beef cattle feedlot, *Atmos. Environ.*, 43, 6091–6099, <https://doi.org/10.1016/j.atmosenv.2009.08.045>, 2009.
- 520 Townsend-Small, A. E., Botner, C., Jimenez, K. L., Schroeder, J. R., Blake, N. J., Meinardi, S., Blake, D. R., Sive, B. C., Bon, D., Crawford, J. H., Pfister, G., and Frank, F. M.: Using stable isotopes of hydrogen to quantify biogenic and thermogenic atmospheric methane sources: A case study from the Colorado Front Range Amy, *Geophys. Res. Lett.*, 31, 1–8, <https://doi.org/10.1002/2013GL058740>.Received, 2016.



- United States Department of Agriculture [USDA]: Colorado Annual Bulletin Colorado Agricultural Statistics, National Agricultural Statistics Service 1, pp. 1–58, 2018.
- 525 Yacovitch, T. I., Herndon, S. C., Roscioli, J. R., Floerchinger, C., McGovern, R. M., Agnese, M., Pétron, G., Kofler, J., Sweeney, C., Karion, A., Conley, S. A., Kort, E. A., Nöhle, L., Fischer, M., Hildebrandt, L., Koeth, J., McManus, J. B., Nelson, D. D., Zahniser, M. S., and Kolb, C. E.: Demonstration of an Ethane Spectrometer for Methane Source Identification, *Environ. Sci. Technol.*, 48, 8028–8034, <https://doi.org/10.1021/es501475q>, 2014.
- Yacovitch, T. I., Daube, C., Vaughn, T. L., Bell, C. S., Roscioli, J. R., Knighton, W. B., Nelson, D. D., Zimmerle, D., Pétron, G., and Herndon, S. C.: Natural gas facility methane emissions: measurements by tracer flux ratio in two US natural gas producing basins, *Elementa: Science of the Anthropocene*, 5, <https://doi.org/10.1525/elementa.251>, 69, 2017.
- 530 Zimmerle, D., Duggan, G., Vaughn, T., Bell, C., Lute, C., Bennett, K., Kimura, Y., Cardoso-Saldaña, F. J., and Allen, D. T.: Modeling air emissions from complex facilities at detailed temporal and spatial resolution: The Methane Emission Estimation Tool (MEET), *Science of the Total Environment*, 824, <https://doi.org/10.1016/j.scitotenv.2022.153653>, 2022.
- 535 *Supplement*. The supplement related to this article is available online at: <https://doi.org/10.5194/jn-0-1-2022-supplement>.